

THE MECHANICAL GREENHOUSE: BURIAL OF HEAT BY TURBULENCE IN HOT JUPITER ATMOSPHERES

ANDREW N. YODIN¹ AND JONATHAN L. MITCHELL²

¹ Canadian Institute for Theoretical Astrophysics, University of Toronto, 60 St. George Street, Toronto, Ontario M5S 3H8, Canada

² Department of Earth & Space Sciences and Department of Atmospheric and Oceanic Sciences, University of California Los Angeles, 595 Charles Young East Drive, Los Angeles, CA 90095-1567, USA

Received 2010 June 8; accepted 2010 August 2; published 2010 September 7

ABSTRACT

The intense irradiation received by hot Jupiters suppresses convection in the outer layers of their atmospheres and lowers their cooling rates. “Inflated” hot Jupiters, i.e., those with anomalously large transit radii, require additional sources of heat or suppressed cooling. We consider the effect of forced turbulent mixing in the radiative layer, which could be driven by atmospheric circulation or by another mechanism. Due to stable stratification in the atmosphere, forced turbulence drives a downward flux of heat. Weak turbulent mixing slows the cooling rate by this process, as if the planet were irradiated more intensely. Stronger turbulent mixing buries heat into the convective interior, provided the turbulence extends to the radiative–convective boundary. This inflates the planet until a balance is reached between the heat buried into and radiated from the interior. We also include the direct injection of heat due to the dissipation of turbulence or other effects. Such heating is already known to slow planetary cooling. We find that dissipation also enhances heat burial from mixing by lowering the threshold for turbulent mixing to drive heat into the interior. Strong turbulent mixing of heavy molecular species such as TiO may be necessary to explain stratospheric thermal inversions. We show that the amount of mixing required to loft TiO may overinflate the planet by our mechanism. This possible refutation of the TiO hypothesis deserves further study. Our inflation mechanism requires a deep stratified layer that only exists when the absorbed stellar flux greatly exceeds the intrinsic emitted flux. Thus, it would be less effective for more luminous brown dwarfs and for longer period gas giants, including Jupiter and Saturn.

Key words: diffusion – opacity – planet–star interactions – planets and satellites: atmospheres – radiative transfer – turbulence

Online-only material: color figures

1. INTRODUCTION

Hot Jupiters—giant planets receiving intense irradiation from their host stars—are the best characterized class of exoplanets. Their proximity to their host star yields frequent transits of and occultations by their host star that are observed over a range of wavelengths. Two remarkable features of hot Jupiters are their inflated radii and the variety of infrared emission signatures, some of which have been interpreted to reveal stratospheric thermal inversions.

Many hot Jupiters have larger radii than standard cooling models predict, even with the intense irradiation from the host stars included in the radiative transfer. This implies a mechanism that injects heat into and/or retards the loss of heat from the planets’ interiors. See Fortney et al. (2009) for a review of proposed mechanisms.

Guillot & Showman (2002, hereafter GS02) argued that atmospheric winds, driven by intense irradiation, could explain inflated radii. In their model, the kinetic energy of the winds dissipates as heat below the penetration depth of starlight. However, the energy need not be deposited into the convective interior (a common misconception). Dissipating energy in outer radiative layers suffices to delay planetary contraction. Turbulence, which the winds can trigger via Kelvin–Helmholtz instabilities, is an efficient mechanism to dissipate kinetic energy (Li & Goodman 2010). MHD drag is an alternative dissipation mechanism provided weather-layer winds extend to the high pressure, metallic zone of hydrogen (Perna et al. 2010; Batygin & Stevenson 2010).

Thermal inversions, i.e., regions where the atmospheric temperature rises with height, may also implicate turbulent

mixing in hot Jupiter atmospheres. Transit spectra of several hot Jupiters have been interpreted as being thermally inverted (Richardson et al. 2007; Burrows et al. 2007; Knutson et al. 2010). These observations appear to confirm the prediction of Hubeny et al. (2003) that molecular absorbers, mainly TiO, in the stratosphere could generate inversion layers. However, vapor phase TiO could rain out of the upper atmosphere if it condenses in cold traps. Turbulent mixing can counteract this settling.

Spiegel et al. (2009, hereafter S09) showed that eddy diffusion coefficients³ of $K_{zz} \approx 10^7\text{--}10^{11} \text{ cm}^2 \text{ s}^{-1}$ are needed to maintain sufficient stratospheric TiO for thermal inversions. The range of K_{zz} values accounts for the varying extent of cold traps in planets with different thermal profiles and the size of grains that condense. S09 argued that the need for strong mixing renders the TiO hypothesis “problematic,” pending improved estimates of K_{zz} . One goal of our study is to determine if large K_{zz} values are energetically problematic.

Sulfur has also been proposed as a high-altitude absorber. Photochemical models of sulfur abundances (Zahnle et al. 2009) also include turbulent mixing at a strength $K_{zz} \approx 10^7 \text{ cm}^2 \text{ s}^{-1}$, though the dependence on K_{zz} is unclear. Eddy diffusion is also used in brown dwarf models to explain disequilibrium chemical abundances (Griffith & Yelle 1999; Hubeny & Burrows 2007).

Turbulence not only mixes chemical species, it also transports heat. This paper develops a model that includes this turbulent heat flux in the radiative layers of hot Jupiters. While convection drives an outward flux of energy, forced turbulence in stably stratified regions drives a downward flux of energy. This effect

³ Eddy diffusion models small-scale turbulent processes in analogy to molecular diffusion, with tracers fluxed down their mean gradients.

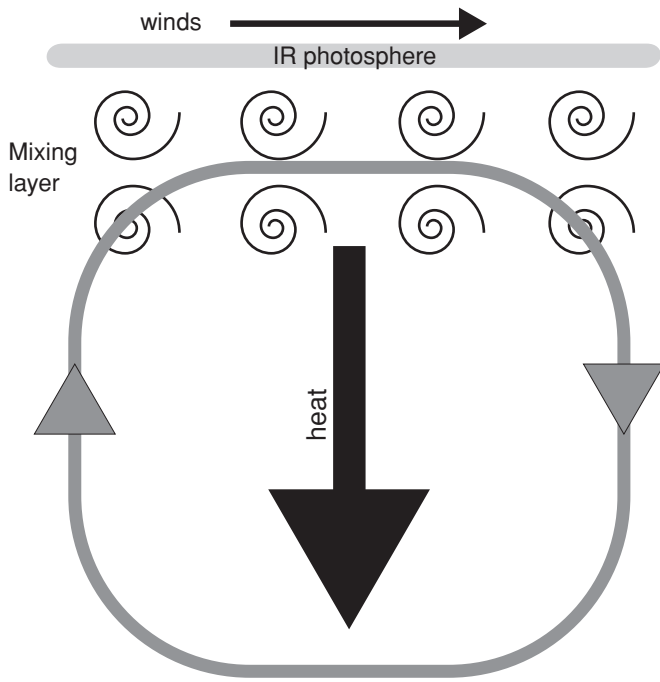


Figure 1. Schematic of the mechanical greenhouse effect to inflate hot Jupiters. A downward flux of heat (large black arrow) is driven by turbulence in the convectively stable “mixing layer” and deposited in the deep interior. This downward flux can balance or even exceed the convective losses (gray overturning arrows). Atmospheric circulation (“winds”) launched near the photosphere drive turbulence in the mixing layer. Other mechanisms, such as nonlinear gravity wave interactions, could also drive the turbulent flux.

is distinct from—though it accompanies—the dissipation of turbulence as heat, which we also include.

By altering the flow of energy, we change the cooling and contraction rates of hot Jupiters. For modest levels of turbulent diffusion, the outward radiative flux is partially offset by the downward flux of mechanical energy. This reduces the net cooling flux from the convective interior, which self-consistently pushes the radiative–convective boundary (RCB) to higher pressure.⁴

For sufficiently strong eddy diffusion, the downward flux of energy exceeds the outward radiative flux that a planet of fixed entropy can provide. In this case, the turbulent heat flux flows into the convective interior, increasing the internal entropy, and inflating the planet. A schematic of this mechanism is shown in Figure 1. Because higher entropy planets are more intrinsically luminous, inflation leads to an equilibrium between turbulent heat burial and radiative losses.

Our mechanism bears some resemblance to the runaway greenhouse. In the latter, the atmosphere is composed of a greenhouse gas in vapor pressure equilibrium with a large, surface volatile reservoir. The cooling emission to space emanates from a pressure $\sim g/\kappa$, with surface gravity g and (Rosseland mean) opacity κ . The emission is independent of the surface temperature for optically thick atmospheres. Vapor pressure equilibrium determines the temperature at the emission level, thus limiting the cooling radiation that the atmosphere can achieve (Kobayashi 1967; Ingersoll 1969). If the absorbed sunlight exceeds this limiting cooling emission, the surface temperature increases until either the volatile reservoir is depleted or the atmosphere becomes sufficiently transparent to the surface

blackbody emission. The role of limiting cooling flux in the runaway greenhouse is played in our mechanism by the cooling flux of the core. The role of absorbed sunlight is played by the downward, mechanical flux of energy. If the latter exceeds the former, the planet heats up by increasing the core entropy until energy balance can be achieved. The analogy is somewhat incomplete, however, in that the traditional runaway greenhouse involves a radiative-thermodynamic feedback which does not exist in our mechanism.

This paper is organized as follows. In Section 2, we review standard radiative equilibrium (RE) models. We add turbulent heat transport and energy injection to our model in Section 3. We derive our mixing length formulae for the turbulent transport of heat in Section 3.1 and present the model equations and our solution methods in Section 3.2. We provide a prescription relating turbulent diffusion and dissipation in stratified atmospheres in Section 3.3. We present and analyze our model results in Section 4. We first treat constant diffusion (partly to connect with S09) and ignore energy dissipation in Section 4.1. We then add complexity by considering a spatially varying K_{zz} in Section 4.2 and including energy dissipation in Section 4.3. We discuss consequences of changing the opacity law in Section 4.4. We compare our results to dynamical simulations of atmospheric circulation in Section 5.1 and to the TiO diffusion needed for thermal inversions in Section 5.2. We summarize our results and their implications in Section 6.

2. STANDARD ATMOSPHERIC MODELS

We start with a review of the standard radiative transfer approximations used in this work (Section 2.1) and apply them to RE solutions (Section 2.2). We will introduce our notation and parameter choices. Arras & Bildsten (2006, hereafter AB06) present a similar analytic model, which they compare to global models with detailed opacities and equation of state (EOS).

2.1. Radiative Transfer

Our goal is to understand energy balance. We focus on the deep atmosphere which is optically thick both to incoming stellar irradiation and the planet’s emitted flux. Here, the equation of radiative diffusion

$$\frac{dT}{dP} = \frac{F_{\text{rad}}}{k_{\text{rad}}} \quad (1)$$

relates the outgoing radiative flux F_{rad} to the variation of temperature T with pressure P via the radiative diffusion coefficient

$$k_{\text{rad}} = \frac{16\sigma T^3 g}{3\kappa}, \quad (2)$$

where σ is the Stephan–Boltzmann constant. Hydrostatic balance, $dP/dz = -\rho g$, allows pressure to replace height z as the vertical coordinate, with ρ the atmospheric density. We hold gravity g constant, invoking the plane-parallel approximation for thin atmospheres.

For the Rosseland mean opacity, our calculations will use a power law,

$$\kappa = \kappa_1 P^\alpha T^\beta \equiv \kappa_o \left(\frac{P}{P_{\text{kb}}}\right)^\alpha \left(\frac{T}{T_{2\text{k}}}\right)^\beta. \quad (3)$$

The two forms are equivalent, with the constant κ_1 being more compact, while κ_o has units of opacity and is normalized to $P_{\text{kb}} = 1$ kbar and $T_{2\text{k}} = 2000$ K. Unless stated otherwise, calculations will use $\kappa \propto P$, i.e., $\alpha = 1, \beta = 0$ as

⁴ For simplicity, we will describe convectively stable regions as “radiative,” even when we include the transport of heat by both turbulence and radiation.

a rough approximation to collision induced molecular opacity. Our normalization choice of $\kappa_o = 0.18 \text{ cm}^2 \text{ g}^{-1}$ will be justified below (Section 2.2). We discuss alternate opacity laws in Section 4.4. While realistic opacities are only well approximated by power laws over a limited range, this considerable simplification is useful for developing intuition.

At the top of our atmosphere, we set the temperature to T_{deep} , an approach used in AB06 and advocated by Iro et al. (2005). This approach is valid when the incident stellar flux exceeds the emitted radiation, resulting in a deep isothermal region at the top of the optically thick atmosphere. In this physical situation, the precise location of the upper boundary is not important, as we explain further in Section 2.2. We point the reader to Hansen (2008) and Guillot (2010) for sophisticated analytic treatments of RE, which are very useful for interpreting computational models. Note that some (Baraffe et al. 2003) but not all (Seager & Sasselov 2000) detailed radiative transfer solutions show an extended isotherm in hot Jupiter atmospheres. One difference between models is the choice of non-gray opacities, which affects the depths at which starlight in different frequency intervals is absorbed.

The incident stellar flux averaged over the full planetary surface, $F_{\text{irr}} \equiv \sigma T_*^4$, gives a characteristic temperature

$$T_* \approx 2000 \text{ K} \frac{L_{*,\odot}^{1/4}}{M_{*,\odot}^{1/6} P_{\text{day}}^{1/3}} \quad (4)$$

where stellar mass and luminosity, $M_{*,\odot}$ and $L_{*,\odot}$ are normalized to solar values, and the orbital period P_{day} is normalized to a (24 hr) day. Horizontal temperature gradients are important for driving winds in the weather layer. However, these winds efficiently smooth temperature gradients at pressures \gtrsim bar, where timescales for advection are shorter than for radiative losses (Showman et al. 2009a). Thus, one-dimensional models are appropriate for basic considerations of energy balance.

Because the planet is not a perfect blackbody, T_{deep} may not match T_* . Greenhouse or anti-greenhouse effects depend on the relative transparency of the atmosphere to stellar and emitted longwave radiation. (To be clear, we are now referring to standard radiative effects, not the mechanical greenhouse.) If incoming starlight penetrates below the infrared photosphere, then the greenhouse effect gives $T_{\text{deep}} > T_*$. If, however, significant incoming radiation is absorbed above the photosphere, a stratospheric thermal inversion gives $T_{\text{deep}} < T_*$. See Hubeny et al. (2003) for a more quantitative analysis. In most of our examples, we adopt $T_{\text{deep}} = 1500 \text{ K}$, as appropriate for short (~ 1 day) orbital periods with a thermal inversion, or for longer periods with no thermal inversion, a greenhouse effect, and/or a more luminous host star.

Giant planets, including hot Jupiters, become unstable to convection at depth. The lapse rate of the atmosphere

$$\nabla \equiv \frac{d \ln T}{d \ln P} = \frac{3\kappa P}{16g} \frac{F_{\text{rad}}}{\sigma T^4} \quad (5)$$

characterizes its stability, and the final equality follows from Equation (1). Convection occurs where $\nabla > \nabla_{\text{ad}}$. We set $\nabla_{\text{ad}} = 2/7$, the adiabatic index of an ideal diatomic gas. In reality, non-ideal interactions lower ∇_{ad} at the high pressures of exoplanet atmospheres and promote convection. At the top the atmosphere, where the optical depth $\tau = \kappa P/g \approx 1$ and $F_{\text{rad}} \ll \sigma T_{\text{deep}}^4$, Equation (5) shows that $\nabla \ll 1$ and the atmosphere is indeed stable and nearly isothermal. For reasonable opacity choices, ∇

increases with depth and gives a transition to convection (even under the ideal gas approximation).

In convective regions, we set $\nabla = \nabla_{\text{ad}}$, i.e., an adiabatic profile with $T \propto P^{\nabla_{\text{ad}}}$. The efficiency of convective energy transport makes the modest super-adiabaticity negligible. The level of the adiabat is determined by the internal entropy. A global calculation of entropy is beyond our illustrative scope. Instead, motivated by Hubbard (1977), we label our adiabats by T_1 , the temperature it would have at $P_1 = 1$ bar pressure, even though the adiabat likely does not extend to such a low pressure. We define a reference entropy (per unit mass) S_{ref} , corresponding to $T_1 = 250 \text{ K}$. Relative entropy values for different T_1 are then computed as

$$\Delta S \equiv S - S_{\text{ref}} = C_P \ln(T_1/250 \text{ K}), \quad (6)$$

where the specific heat (at constant pressure) $C_P = R/\nabla_{\text{ad}}$ is assumed constant. For the gas constant $R = k_B/(\mu m_p)$, we use a mean molecular weight $\mu = 2.34$ times the proton mass m_p .

The stable atmosphere matches smoothly onto the convective adiabat at the RCB. Since the temperature T_c and pressure P_c at the RCB lie on the interior adiabat we require

$$T_1 = T_c \left(\frac{P_1}{P_c} \right)^{\nabla_{\text{ad}}}. \quad (7)$$

The location of the RCB is crucial for global evolution. The secular cooling of the convective interior is determined by the radiative flux, F_c , leaving the RCB. Combining Equations (3), (5), and then (7) at the RCB gives

$$F_c = \frac{\nabla_{\text{ad}} 16g\sigma T_c^{4-\beta}}{3\kappa_1 P_c^{1+\alpha}} \quad (8)$$

$$= \frac{\nabla_{\text{ad}} 16g\sigma}{3\kappa_1} \left(\frac{T_1}{P_1^{\nabla_{\text{ad}}} P_c^{\nabla_{\infty} - \nabla_{\text{ad}}}} \right)^{4-\beta} \propto \frac{T_1^4}{P_c^{6/7}}, \quad (9)$$

with

$$\nabla_{\infty} \equiv (1 + \alpha)/(4 - \beta) = 1/2. \quad (10)$$

Core flux increases with the interior entropy.⁵ Pushing the RCB to higher pressures decreases the core flux if $\nabla_{\infty} > \nabla_{\text{ad}}$. This condition is satisfied for our opacity choice and is generally required for a transition to convection (as we will show shortly). We emphasize that the dependence of F_c on P_c is independent of the mechanism that changes P_c , though previous works have mostly considered irradiation. These basic considerations are useful in interpreting numerical studies of planetary cooling histories and radii evolution (Burrows et al. 2000; Baraffe et al. 2003; Chabrier et al. 2004).

2.2. Radiative Equilibrium Solutions

We now apply the two approximations of RE to the stable layer. First, radiation is the only relevant energy transport mechanism. Thus, F_{rad} in Equation (1) is the total flux of energy. Second, the flux is constant through the radiative layer with $F_{\text{rad}} = F_c$, the flux from the convective interior. This assumes that local (thermal) energy release is negligible.

Figure 2 plots radiative equilibrium atmospheres for $\kappa \propto P$, with two values of T_{deep} matched on to interior adiabats

⁵ The numerical scaling in Equation (9) ignores the effect that higher entropy would lower gravity by inflating the planet. This effect cancels when computing the total luminosity, which is ultimately more important.

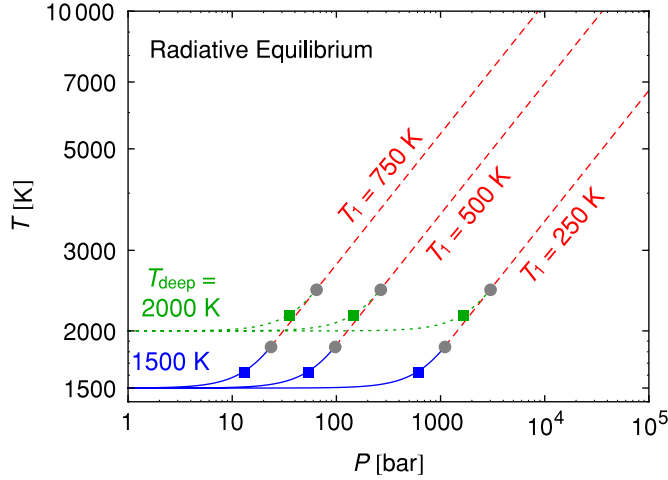


Figure 2. Radiative equilibrium (RE) atmospheres with deep isotherms of $T_{\text{deep}} = 1500$ K (blue curves) and 2000 K (dotted green curves) matched onto internal adiabats (dashed red curves) with entropy increasing from bottom to top. Gray dots mark the location (T_c and P_c) of the radiative–convective boundary (RCB) and squares show P_{deep} , where $\nabla = \nabla_{\text{ad}}/2$. (A color version of this figure is available in the online journal.)

labeled by T_1 . We obtain analytic RE solutions by integrating Equation (1) with $F_{\text{rad}} = F_c$ and $T = T_{\text{deep}}$ at $P = 0$ to get

$$T = T_{\text{deep}} \left[1 + \frac{\nabla_{\text{ad}}}{\nabla_{\infty} - \nabla_{\text{ad}}} \left(\frac{P}{P_c} \right)^{1+\alpha} \right]^{1/(4-\beta)}. \quad (11)$$

This solution uses Equation (8) and we have imposed the requirement $T(P_c) = T_c$ to find

$$T_c = T_{\text{deep}} \left(\frac{\nabla_{\infty}}{\nabla_{\infty} - \nabla_{\text{ad}}} \right)^{1/(4-\beta)}. \quad (12)$$

A valid solution—one that transitions to convection—thus requires $\nabla_{\infty} > \nabla_{\text{ad}}$ and $\alpha > -1$ (which together assure $\beta < 4$). As Figure 2 shows, T_c increases with T_{deep} but is independent of the interior entropy.

The RCB sinks to larger pressure as entropy decreases or as T_{deep} increases,

$$P_c = k_{\nabla} P_1 \left(\frac{T_{\text{deep}}}{T_1} \right)^{1/\nabla_{\text{ad}}}, \quad (13)$$

which follows from Equations (7) and (12) with the constant

$$k_{\nabla} \equiv \left(\frac{\nabla_{\infty}}{\nabla_{\infty} - \nabla_{\text{ad}}} \right)^{\nabla_{\infty}/[\nabla_{\text{ad}}(1+\alpha)]} \approx 2.1.$$

The core flux for RE atmospheres follows from Equations (8), (12), and (13) as

$$F_c = k_F \frac{g}{\kappa_1} \left(\frac{T_1}{T_{\text{deep}}^{1-\nabla_{\text{ad}}/\nabla_{\infty}}} \right)^{(1+\alpha)/\nabla_{\text{ad}}} \propto \frac{T_1^7}{T_{\text{deep}}^3}. \quad (14)$$

This gives the well-known result that increased irradiation reduces the cooling of the planet, while higher entropy planets are more luminous. The constant

$$k_F \equiv \frac{16\sigma \nabla_{\text{ad}}}{3P_1^{1+\alpha}} \left(1 - \frac{\nabla_{\text{ad}}}{\nabla_{\infty}} \right)^{\nabla_{\infty}/\nabla_{\text{ad}}-1}.$$

Equation (14) is consistent with, but more specific than, Equation (9) in assuming that RE sets the location of P_c .

We chose the parameters for Figure 2—used throughout this work—by roughly matching the analytic solutions to more detailed hot Jupiter models, as in AB06.

We constrain the entropy parameter T_1 by appealing to the typical $P_c \approx 1$ kbar location of the RCB in hot Jupiters with modest, i.e., Jovian, entropies. With $T_1 = 260$ K, we reproduce a 1 kbar RCB for $T_{\text{deep}} = 1500$ K. We also consider larger values of T_1 to describe more inflated planets, but keep $P_c \gg 1$ bar.

The normalization of the opacity determines the core flux.⁶ Requiring $F_c = \sigma(100 \text{ K})^4$ for the standard parameters and $P_c = 1$ kbar gives $\kappa_0 = 0.18 \text{ cm}^2 \text{ g}^{-1}$ for $g = 10^3 \text{ cm}^2 \text{ s}^{-1}$. We emphasize that this is not a realistic opacity law (in particular it is too low at small pressures). We are merely choosing parameters that allow the simple analytic model to mimic properties of more detailed hot Jupiter models.

The lapse rate for RE solutions is (from Equation (11))

$$\nabla = \nabla_{\text{ad}} \frac{(P/P_c)^{1+\alpha}}{\left(1 - \frac{\nabla_{\text{ad}}}{\nabla_{\infty}} \right) + \frac{\nabla_{\text{ad}}}{\nabla_{\infty}} (P/P_c)^{1+\alpha}}, \quad (15)$$

demonstrating that $\nabla = \nabla_{\text{ad}}$ at $P = P_c$ and that the solution becomes isothermal $\nabla \rightarrow 0$ at low pressures. Smooth opacity laws give a monotonic increase in ∇ with P . Opacity windows give more complicated profiles of ∇ , including multiple zones of convection (see Section 4.4).

We define P_{deep} , the effective depth of the isothermal layer, as the location where $\nabla = \nabla_{\text{ad}}/2$. This occurs at

$$P_{\text{deep}} = \left(\frac{\nabla_{\infty} - \nabla_{\text{ad}}}{2\nabla_{\infty} - \nabla_{\text{ad}}} \right)^{1/(1+\alpha)} P_c \approx 0.55 P_c. \quad (16)$$

Our definition of P_{deep} differs from AB06, who define P_{deep} as a characteristic scale that might exceed P_c .

We now revisit the validity of applying the boundary condition $T = T_{\text{deep}}$ at $P = 0$. Due to the isothermal layer at low pressures, applying the boundary condition at any $P \ll P_{\text{deep}}$ gives indistinguishable solutions. However, solutions are only physically valid in optically thick regions, for $P \gg P_{\text{thick}} \sim g/\kappa_{\text{min}} \sim 10 \text{ mbar} [\kappa_{\text{min}}/(0.1 \text{ cm}^2 \text{ g}^{-1})]^{-1}$. The relevant opacity κ_{min} is the smaller of the opacities to starlight and emitted radiation near P_{thick} . Indeed, the penetration of starlight below the infrared photosphere can push the top of the isotherm to ~ 1 bar (Guillot 2010). As long as $P_{\text{thick}} \ll P_{\text{deep}}$, solutions are physically consistent below P_{thick} .

3. ENERGETICS OF TURBULENT RADIATIVE LAYERS

We now generalize the RE model to include two effects. First, we allow for turbulent eddies to drive an advective heat flux F_{eddy} . The total flux

$$F = F_{\text{rad}} + F_{\text{eddy}} \quad (17)$$

includes the radiative and eddy contributions. Second, we allow for the release of energy at a rate ϵ . In steady state, this heating is balanced by cooling from the divergence of the total flux,

$$\frac{dF}{dP} = -\frac{\epsilon}{g}. \quad (18)$$

⁶ Remarkably, κ_0 does not affect the location of the RCB along a given adiabat, only T_{deep} and the power laws are required. Over long times though, the opacity at the RCB affects entropy evolution and thereby RCB location.

Sources of ϵ include the viscous dissipation of turbulence (Section 4.3), breaking waves (Showman et al. 2009a), and ohmic dissipation (Batygin & Stevenson 2010).

While Equation (1) still describes the radiative flux, F_{rad} , it is no longer constant with height. The fractional contribution of F_{rad} to the total flux can vary, and the total flux itself can vary. To proceed further we require a model for F_{eddy} and ϵ .

3.1. Turbulent Heat Transport

We derive F_{eddy} using basic elements of mixing length theory. This theory is usually applied to convectively unstable regions, but instead we apply it to forced turbulence in convectively stable regions. We will show that in this case the energy flux is inward. We leave the forcing mechanism of turbulent motions unspecified and their strength a free parameter.

We consider parcels of gas which conserve entropy and maintain pressure equilibrium with their surroundings as they exchange positions over a vertical distance ℓ and then dissolve. These parcels contain excess heat $\delta q = \rho C_P \delta T$ with

$$\begin{aligned} \delta T &= \left(\frac{dT}{dz} \Big|_{\text{ad}} - \frac{dT}{dz} \right) \ell \\ &= -\frac{\ell T}{C_P} \frac{dS}{dz}, \end{aligned} \quad (19)$$

where δf gives the difference of any quantity f between the parcel and its surroundings. For stable stratification ($dS/dz > 0$), rising parcels ($\ell > 0$) cool down and sinking parcels heat up. We express the heat flux, $F_{\text{eddy}} = w \delta q$ with w the characteristic eddy speed, in terms of the turbulent diffusion, $K_{zz} = w\ell$, as

$$\begin{aligned} F_{\text{eddy}} &= -K_{zz} \rho T \frac{dS}{dz} \\ &= -K_{zz} \rho g \left(1 - \frac{\nabla}{\nabla_{\text{ad}}} \right). \end{aligned} \quad (20)$$

The flux is always negative for stable stratification. It vanishes at the RCB where $dS/dz = 0$ (and $\nabla = \nabla_{\text{ad}}$). We do not model overshoot, which could allow energy exchange (in either direction) between convectively stable and unstable zones. In the upper isothermal regions $F_{\text{eddy}} \propto -K_{zz} P$, declines in magnitude with height, unless K_{zz} increases with height to compensate, as we will consider in Section 4.2.

The above assumption that parcels conserve entropy assumes a radiative cooling time longer than the eddy turnover time. We are ignoring radiative losses during eddy motion in this work, because we consider optically thick regions with long cooling times. This assumption will eventually break down in optically thin regions, notably the inversion layer itself, which is strongly stratified. Whether eddy fluxes affect the structure of the inversion layer is left to future work.

To understand the energetics of F_{eddy} , we analyze its divergence, which describes cooling and (when negative) heating,

$$\frac{dF_{\text{eddy}}}{dz} = K_{zz} \frac{\rho g}{R} \frac{dS}{dz} - K_{zz} \rho T \frac{d^2 S}{dz^2} - \frac{dK_{zz}}{dz} \rho T \frac{dS}{dz}. \quad (21)$$

The terms on the right-hand side represent cooling rates, $-\delta \dot{q}$, which we relate to rates of work, $\delta \dot{w}$, using the first law, $\delta q = \delta e - \delta w$. Thus, $-\delta \dot{q} = \delta \dot{w} / \nabla_{\text{ad}}$ since the internal energy, $\delta e = \rho C_V \delta T = (1 - \nabla_{\text{ad}}) \delta q$ with $C_V = C_P - R$. The first term in Equation (21) arises from buoyant work $\delta \dot{w}_B = \delta \rho g w = K_{zz} \rho g (dS/dz) / C_P$, where $\delta \rho / \rho = -\delta T / T$

by pressure equilibrium. The first term on the right-hand side of Equation (21) is thus $-\delta \dot{q}_B = \delta \dot{w}_B / \nabla_{\text{ad}}$. This buoyant cooling will be evident in the stratified regions ($P < P_{\text{deep}}$) of Figure 6.

The second term represents the tendency of mixing to heat by filling in entropy minima (for $d^2 S / dz^2 > 0$). More specifically, it arises from compressional work, which vanishes for a constant entropy gradient because the work done on rising and sinking parcels cancels out. For varying dS/dz consider two parcels that arrive at z , one from above and one from below. Compressional work is done on the parcels at a rate

$$P \nabla \cdot \mathbf{v}_{\pm} = -\frac{P}{\rho} \frac{\delta \rho_{\pm}}{\delta t} = \mp \frac{P \ell}{C_P} \frac{dS}{dz} \Big|_{z \pm \ell} \frac{w}{\ell}, \quad (22)$$

where the top (bottom) sign refers to sinking (rising) parcels, $\nabla \cdot \mathbf{v}$ is a velocity divergence, and $\delta t = \ell / w$ gives the expansion rate. The net work is the sum of these terms, $\delta \dot{w}_C = -\nabla_{\text{ad}} K_{zz} \rho T d^2 S / dz^2$. We identify the second right-hand side term in Equation (21) as $-\delta \dot{q}_C = \delta \dot{w}_C / \nabla_{\text{ad}}$. This compressional heating dominates in deeper regions ($P > P_{\text{deep}}$) of Figure 6. The third and final term represents a flux imbalance that arises from non-uniform eddy diffusion as in Section 4.2.

3.2. Model Equations and Self-similar Solution Technique

Our atmospheric model is described by Equations (1), (17), (18), and (20) which reduce to the following pair of coupled ordinary differential equations (ODEs)

$$\frac{dT}{dP} = \frac{F + F_{\text{iso}}}{k_{\text{rad}} + F_{\text{iso}} P / (\nabla_{\text{ad}} T)} \quad (23)$$

$$\frac{dF}{dP} = -\frac{\epsilon}{g} \quad (24)$$

where

$$F_{\text{iso}} \equiv K_{zz} \rho g \quad (25)$$

is (minus one times) the isothermal limit of the eddy flux. The thermal profile in Equation (23) describes the combined effects of radiative and eddy fluxes. Ignoring mixing ($F_{\text{iso}} \rightarrow 0$) recovers standard radiative diffusion of Equation (1). Strong mixing ($F_{\text{iso}} \rightarrow \infty$) creates an isentropic profile ($\nabla \rightarrow \nabla_{\text{ad}}$).

Solving the coupled ODEs for T and F requires prescriptions for K_{zz} and ϵ and boundary conditions. As with the RE solutions, we fix T_{deep} at the top of the atmosphere and match onto an adiabat with a given T_1 at the bottom. This matching generally requires iterative techniques. We avoid this complication by finding self-similar solutions. This technique is only possible because of the idealizations—notably power-law opacities and ideal gas EOS—described in Section 2.1.

To find self-similar solutions, we normalize all quantities to their value at the RCB. As with the analytic RE solutions, we do not know where the RCB is located until we find the solution. We integrate outward from the RCB with trivial boundary conditions: the dimensionless T and F are unity.

We set the strength of diffusion not with a physical value for K_{zz} , but by the parameter

$$\psi_c = \frac{K_{zz} \rho_c g}{F_c}, \quad (26)$$

the ratio of F_{iso} to $F = F_{\text{rad}}$ at the RCB. For dissipation, we must similarly specify $\epsilon P / (g F)$ at the RCB. See Appendix B for details.

To get a physical solution, we scale a dimensionless solution to any desired value of T_{deep} and T_1 . Setting $T = T_{\text{deep}}$ at $P = 0$, the solution gives T_c at the RCB. Specification of T_1 then fixes P_c via Equation (7). We then determine F_c and K_{zz} via Equations (8) and (26).

3.3. Relating Diffusion and Dissipation

Turbulence that gives rise to diffusion, K_{zz} , will also dissipate at some rate ϵ . We now consider a prescription that sets a lower bound on ϵ from turbulence. We also allow for stronger heating, perhaps from non-turbulent sources.

In a Kolmogorov cascade, the dissipation rate $\epsilon = w^3/\ell$ and the diffusion $K_{zz} = w\ell$ give a simple relation $\epsilon = K_{zz}/t_o^2$, with $t_o = \ell/w$ the turnover time of the dominant eddies. Unfortunately, we lack a reliable model for eddy timescales. Moreover, turbulence in a stratified atmosphere is likely anisotropic and not well described by Kolmogorov scalings. Fortunately, our results are not very sensitive to this limitation, as we will show in subsequent sections. Eddies with long turnover times, $t_o > 1/N$, organize into horizontally extended pancakes, where the squared buoyancy frequency is

$$N^2 = \frac{g^2}{RT} [\nabla_{\text{ad}} - \nabla]. \quad (27)$$

Assuming that the buoyancy frequency sets the relevant timescale, $t_o = 1/N$, gives a dissipation rate

$$\epsilon_{\text{buoy}} \approx K_{zz} N^2. \quad (28)$$

In strongly stratified, isothermal regions the buoyancy is

$$N_{\text{deep}} = g/\sqrt{C_P T_{\text{deep}}} \sim c_s/H \quad (29)$$

with c_s the sound speed and H the scale height. For sub-sonic turbulence with $w \ll c_s$, our prescription gives $\ell \sim w/N \ll H$. This is consistent with the expectation that stratification limits the vertical extent of turbulent structures to less than a scale height. Forced turbulence with $t_o < 1/N$ is also possible. Since this would give even stronger dissipation, we consider ϵ_{buoy} a reasonable lower bound on dissipation for stratified turbulence.

Near the RCB, as $N \rightarrow 0$ it is unreasonable to expect the dissipation to vanish entirely. Thus, we also include a floor to the dissipation

$$\epsilon_o = f_\epsilon K_{zz} N_{\text{deep}}^2 \quad (30)$$

with the dimensionless normalization f_ϵ giving the ratio of ϵ_o to ϵ_{buoy} in isothermal regions. If we use rotation as the other relevant timescale, then the floor would be quite low with $f_\epsilon \sim \Omega^2/N_{\text{deep}}^2 \sim 10^{-3} P_{\text{day}}^{-7/3}$. Our full prescription considers both terms,

$$\epsilon = \epsilon_o + \epsilon_{\text{buoy}}, \quad (31)$$

as discussed in Section 4.3.

4. RESULTS

4.1. Constant Diffusion, No Dissipation

We describe solutions to the atmospheric model of Section 3. We start by considering turbulent mixing with a constant diffusivity K_{zz} and no dissipation, i.e., $\epsilon = 0$. This requires integration of Equation (23). While the decay of turbulence always gives some dissipation, the effect on energetics can be small (as we will show in Section 4.3).

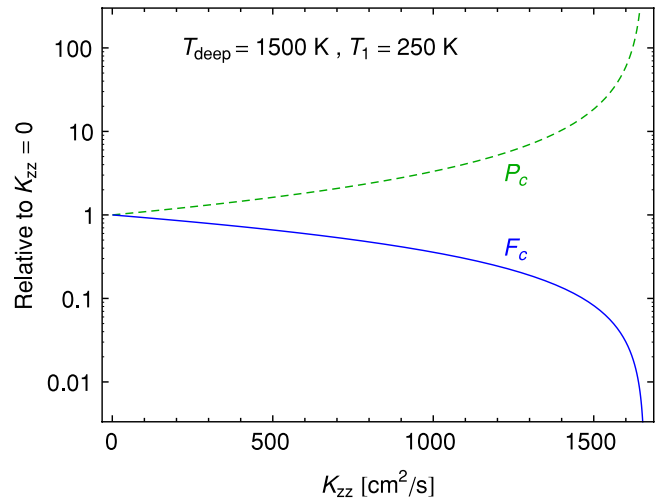


Figure 3. As K_{zz} increases, the RCB moves to high pressure (P_c , dashed green curve) while the core flux (F_c , blue curve) drops. Both diverge at finite $K_{zz} = K_{zz,\text{crit}} \approx 1660 \text{ cm}^2 \text{ s}^{-1}$, when dissipation is ignored ($\epsilon = 0$). This upper limit varies with internal entropy and T_{deep} , as shown in Figure 4. Quantities are plotted relative to the $K_{zz} = 0$ case where $P_c = 1.1 \text{ kbar}$ and $F_c = \sigma(100 \text{ K})^4$. (A color version of this figure is available in the online journal.)

Our main goal is to constrain the amount of turbulent diffusion that can be maintained in convectively stable regions. The simplest and most generous—i.e., allowing the largest levels of turbulent diffusion—constraint comes when we ignore dissipation.

An appeal to energetic balance shows why this should be the case. Recalling that turbulence drives a downward eddy flux, $F_{\text{eddy}} < 0$, in convectively stable regions, we rearrange flux balance as $-F_{\text{eddy}} = F_{\text{rad}} - F$. For a large downward eddy flux, we need the total flux F to be small compared to the outgoing radiative flux. Ignoring dissipation helps in this regard by preventing F from increasing through the layer. Pushing the RCB to high pressure also helps by lowering the constant $F = F_c$ from the RCB. The solutions below show that strong mixing does indeed push the RCB to high pressure.

4.1.1. An Upper Limit to K_{zz}

Figure 3 shows the effect of varying K_{zz} while holding irradiation ($T_{\text{deep}} = 1500 \text{ K}$) and internal entropy ($T_1 = 250 \text{ K}$) fixed. As K_{zz} increases, the downwelling eddy flux pushes the RCB to higher pressures, P_c , and lowers the flux from the interior, F_c . These effects are coupled since $T_c \propto P_c^{-6/7}$ along a fixed adiabat (Equation (9)). Turbulent mixing—like strong stellar irradiation—reduces the planet’s cooling rate.

At a critical value of $K_{zz} = K_{zz,\text{crit}}$, P_c diverges to infinity while F_c drops to zero. This upper limit to diffusion is $K_{zz,\text{crit}} \approx 1660 \text{ cm}^2 \text{ s}^{-1}$ for the adiabat and the T_{deep} chosen in Figure 3. Of course a real planet cannot extend to infinite pressure, to say nothing of the plane-parallel approximation. The point is that our steady state model cannot energetically support $K_{zz} > K_{zz,\text{crit}}$.

Stronger turbulence could in principle exist, since we are saying nothing about what forces turbulence. In a non-equilibrium state with $K_{zz} > K_{zz,\text{crit}}$, the downwelling eddy flux would then increase the internal entropy and inflate the planet.

Figure 4 shows that higher entropy planets have a higher steady state $K_{zz,\text{crit}}$. Thus by inflating the planet, strong mixing brings the planet’s energy balance into equilibrium. An ultimate upper limit to K_{zz} is that the planet not overinflate and exceed its observed radius. The K_{zz} values invoked in S09, from 10^7

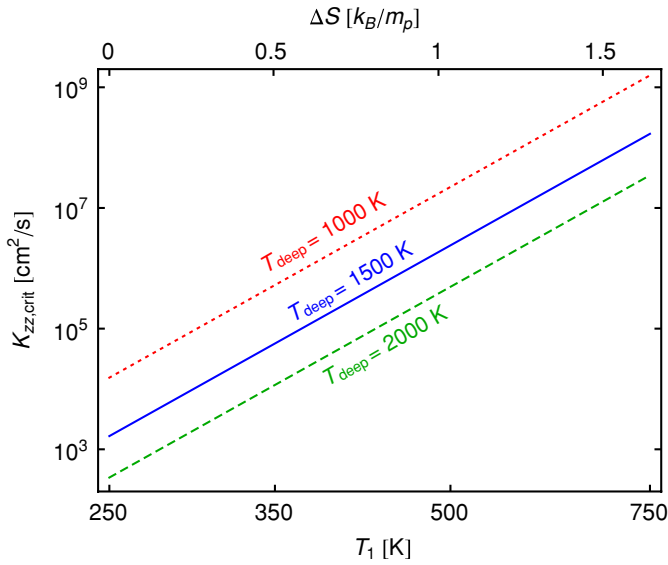


Figure 4. Maximum eddy diffusion in the stable layer ($K_{zz,crit}$) vs. internal entropy for $T_{deep} = 1000, 1500,$ and 2000 K (dotted red, blue, and dashed green curves, respectively). See Equation (32) for analytic fits. Entropy is given in terms of T_1 (Equation (7)) and relative to the $T_1 = 250$ K reference (top axis). (A color version of this figure is available in the online journal.)

to $> 10^{10} \text{ cm}^2 \text{ s}^{-1}$ would imply significant or (on the upper end) excessive inflation. For comparison, AB06 showed (see their Figure 11) that entropy changes of $\Delta S \approx k_B/m_p$ (the scale in our Figure 4) can expand a hot Jupiter’s radius by $\sim 10\%–25\%$. Accurate determination of the maximum K_{zz} allowed for a given planet requires more detailed modeling (including global structure with realistic opacities and EOS) than we perform. However, our results strongly suggest that K_{zz} values invoked in the literature have significant, or even excessive, effects on energetics.

Figure 4 also shows that $K_{zz,crit}$ increases with decreasing T_{deep} . Thus, our constraints on mixing are much more stringent for hot Jupiters than for more distant planets, including Jupiter itself. Recall that thermal inversions lower T_{deep} and that mixing can sustain thermal inversions by keeping opacity sources aloft in the stratosphere. A planet can accommodate strong mixing with some combination of thermal inversions to lower T_{deep} and increased internal entropy. It is hard to predict if thermally inverted planets should be more inflated—due to the presumed presence of turbulence—or less inflated—because lower T_{deep} promotes cooling and inhibits our mechanical greenhouse effect. Observations do not indicate an obvious correlation. Planets with signatures of inversions exhibit varying degrees of inflation. See Miller et al. (2009) for a comparison of observed to model radii of transiting planets.

While strong mixing pushes $P_c \rightarrow \infty$, the depth of the isothermal layer, P_{deep} , is relatively unchanged by mixing. (We explore structure in detail below.) Thus, planets with higher entropy or lower T_{deep} have shallower isothermal layers. Specifically, $P_{deep} \propto (T_{deep}/T_1)^{1/\nabla_{ad}}$ from Equations (13) and (16).

It is hardly surprising that planets which can accommodate more mixing (larger $K_{zz,crit}$) have shallower stratified layers to mix (smaller P_{deep}). In principle, strong mixing could destroy the deep isotherm altogether by pushing P_{deep} to optically thin regions. This probably requires unrealistically large core entropies. Alternatively, as interior temperatures rise, blackbody

emission at depth may find opacity windows at wavelengths longer than the infrared.

4.1.2. Structure and Energetics of Stirred Atmospheres

We now consider the structure and energetic balance of “stirred atmospheres” with $K_{zz} \approx K_{zz,crit}$. We compare these solutions to standard RE atmospheres of Section 2.2 with $K_{zz} = 0$. Since our model is self-similar, the behavior is independent of the parameters (T_1, T_{deep}) chosen for illustration.

Figure 5 (top panel) shows that the temperature profile of the stirred atmosphere is very similar to the RE case. In the stirred atmosphere, the RCB lies at much higher pressure below an extended “pseudo-adiabat,”⁷ which lies very close to the original adiabat. The inset to Figure 5 (top panel) focuses on the region near P_{deep} (which drops slightly to 480 bar from the original 610 bar) where the stirred atmosphere is hotter, by at most 60 K. The stirred atmosphere is slightly colder below 250 bar, though this difference of at most 3 K is not visible. The stirred atmosphere is very modestly thicker, by $0.06 H_{deep}$, where $H_{deep} = RT_{deep}/g \approx 0.008 R_J$.

Figure 5 (bottom panel) plots the lapse rate. Mixing smooths the transition toward the adiabat. The inset shows the smooth decline of $1 - \nabla/\nabla_{ad}$ along the pseudo-adiabat, which gradually reduces the amplitude of the downwelling eddy flux, from Equation (20).

Figure 6 shows that the energetics of the stirred atmosphere differ significantly from the RE case. With $K_{zz} = 0$ there is no eddy flux and the radiative flux is constant down to the RCB, here at $P_c \approx 1.1$ kbar. The stirred atmosphere has a deeper RCB which reduces the core flux significantly. We could push $P_c \rightarrow \infty$ and $F_c \rightarrow 0$ with a 0.1% increase of K_{zz} all the way to $K_{zz,crit}$, but choose not to for visualization.

The radiative and eddy fluxes change with height. Their sum—the total flux—remains constant because we ignore dissipation. Figure 6 shows that the fluxes behave differently above and below P_{deep} , i.e., along the isothermal and pseudo-adiabatic regions, respectively. Along the pseudo-adiabat, the radiative flux declines with depth as $F_{rad} \propto P^{-6/7}$, as we derived for the core flux in Equation (8). The radiative cooling ($dF_{rad}/dP < 0$) in this region balances heating by eddy diffusion ($dF_{eddy}/dP > 0$). Achieving this energetic balance requires only modest changes to the T - P profile. Since F_{eddy} scales as $1 - \nabla/\nabla_{ad}$, it is very sensitive to small changes in ∇ along the pseudo-adiabat (see Equation (20) and the bottom inset of Figure 5).

The energy balance along the isotherm, i.e., above P_{deep} is different. With $\nabla \ll 1$, the eddy flux $F_{eddy} \approx -\rho g K_{zz} \propto -P$ grows in magnitude with depth (a different scaling holds if we vary K_{zz} with height, see Section 4.2). This localized cooling ($dF_{eddy}/dP < 0$) balances radiative heating ($dF_{rad}/dP > 0$). The decline in radiative flux with height again requires only modest changes to the thermal profile. From Equation (5), F_{rad} is sensitive to small changes in $\nabla \ll 1$.

We can now simply estimate $K_{zz,crit}$ using our knowledge that $F_c \rightarrow 0$ and that mixing only modestly changes the RE profile. The transition region near P_{deep} is crucial. Here, the eddy flux reaches its peak negative value $F_{eddy,deep} \approx -\rho_{deep} g K_{zz}/2$. The thermal profile constrains F_{rad} to be roughly $F_c(K_{zz} = 0)$, the core flux of the RE atmosphere. We set $F_{rad,deep} \approx 2F_c(K_{zz} = 0)$ to account for the slightly hotter atmosphere near P_{deep} .

⁷ This is not to be confused with the pseudo-adiabat that describes moist convection in Earth’s atmosphere.

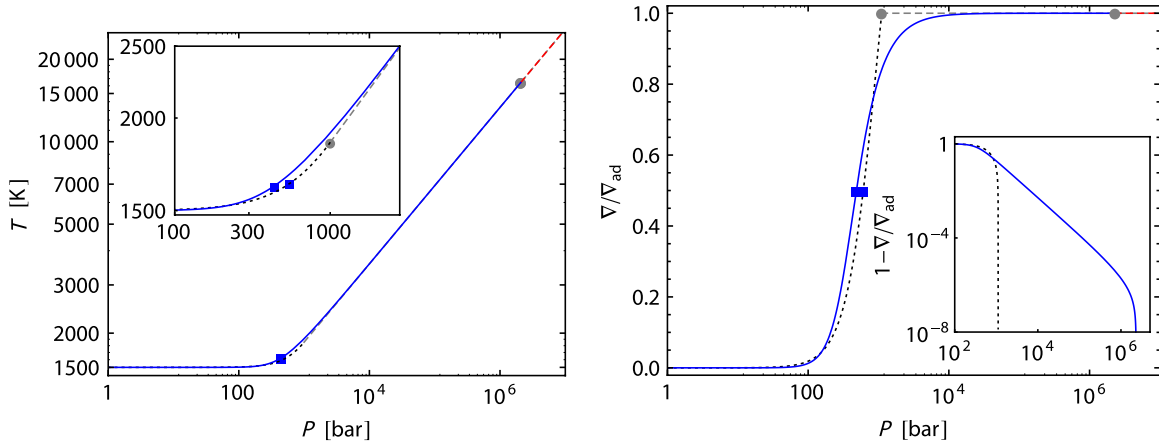


Figure 5. Profiles of a stirred atmosphere (blue curves) with $K_{zz} \approx K_{zz,\text{crit}}$ and no dissipation compared to the RE case with $K_{zz} = 0$ (dotted black curves). Both join an adiabat with $T_1 = 250$ K (dashed red and gray curves). Mixing pushes the RCB (gray dots) to high pressure (which remains finite because K_{zz} is 0.1% below $K_{zz,\text{crit}}$). Left: the temperature profile shows modest changes near P_{deep} (blue squares), as shown in the inset. Right: lapse rate, ∇ , relative to ∇_{ad} . Turbulent diffusion smoothes the transition toward the adiabat. The inset plot of $1 - \nabla/\nabla_{\text{ad}}$ shows the marginal stability of the stirred atmosphere up to high pressures.

(A color version of this figure is available in the online journal.)

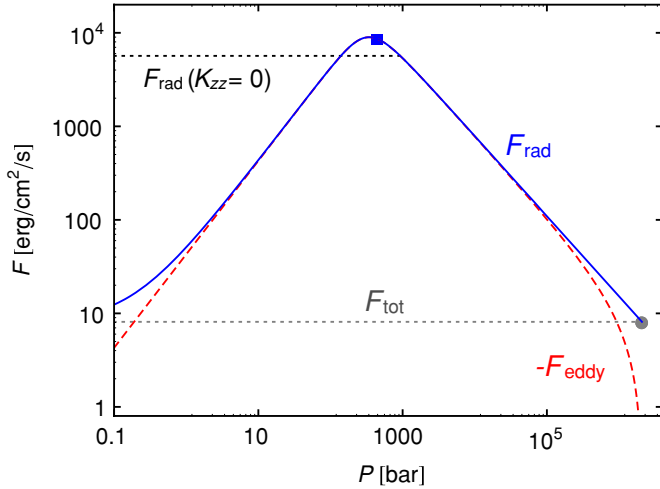


Figure 6. Energetic balance for the profiles in Figure 5. In radiative equilibrium (black dotted curve), the radiative flux is constant. With eddy diffusion and no dissipation the total flux (gray dotted curve) is constant. The radiative flux (blue curve) leaving the interior is low, but F_{rad} first increases and then decreases outward, peaking near P_{deep} (blue square). The downwelling eddy flux (dashed red curve) offsets change to the radiative flux.

(A color version of this figure is available in the online journal.)

Energetic balance, $F_{\text{eddy,deep}} + F_{\text{rad,deep}} = F_c \rightarrow 0$, then gives

$$K_{zz,\text{crit}} \approx \frac{4F_c(K_{zz}=0)}{\rho_{\text{deep}}g} \propto \left(\frac{T_1^{1/\nabla_{\text{ad}}}}{T_{\text{deep}}^{1/\nabla_{\text{ad}}-1/\nabla_{\infty}'}} \right)^{2+\alpha}, \quad (32)$$

where $\nabla_{\infty}' = (2+\alpha)/(5-\beta)$ and our parameters give $K_{zz,\text{crit}} \propto T_1^{21/2}/T_{\text{deep}}^{11/2}$. These scalings agree with the results of Figure 4.

4.2. Spatially Varying K_{zz}

The above analysis (Section 4.1) shows that upper limits on a constant K_{zz} are set by the balance of eddy and radiative fluxes near P_{deep} , which itself scales with internal entropy and T_{deep} . To test the robustness of this finding, we include a depth dependence to $K_{zz} \propto P^{\zeta}$. For winds driven near the photosphere, i.e., the top of our atmospheres, one might expect stronger diffusion

in the upper atmosphere, i.e., $\zeta < 0$. On the other hand, if turbulence is triggered by shear layers with the convective interior, perhaps $\zeta > 0$. As discussed in Section 5.1, detailed dynamical simulations can help determine plausible diffusion profiles.

Figure 7 shows the effect of varying ζ with other parameters fixed (at our standard values of $T_{\text{deep}} = 1500$ K, $T_1 = 250$ K, $\alpha = 1$, and $\beta = 0$ as in, e.g., Figure 3). These plots show the strongest possible mixing, which (as we found for constant K_{zz}) drives the RCB to infinite depths and reduces the core flux to zero.

The maximum mixing near P_{deep} is relatively unchanged, except when the mixing at the top of the atmosphere is quite strong. Quantitatively we compare values of $K_{zz,\text{deep}}$, defined as the maximum value of K_{zz} at a reference pressure $P = 550$ bar, which is P_{deep} of the RE atmosphere. For constant K_{zz} , we found $K_{zz,\text{crit}} = K_{zz,\text{deep}} = 1665 \text{ cm}^2 \text{ s}^{-1}$. For mixing that increases with depth as $\zeta = 0.5, 1.0$, and 1.5 , $K_{zz,\text{deep}}$ declines by a modest 5%, 6%, and 5%, respectively. When mixing declines with depth as $\zeta = -0.5, -1.0$, and -1.4 , $K_{zz,\text{deep}}$ increases by 14%, 58%, and 300%, respectively. We cannot consider models with $\zeta \lesssim -1.5$ because they do not approach an adiabat at depth. The bottom panel of Figure 7 shows that the approach to the adiabat is already quite gradual for $\zeta = -1.4$. We explore this issue further in Appendix A.

The top panel of Figure 7 shows the flux profiles for several ζ values. The plot shows both radiative and eddy fluxes, which obey $F_{\text{rad}} = -F_{\text{eddy}}$ because the net flux, $F \rightarrow 0$, when mixing pushes the RCB to infinite depth. We also plot the radiative flux for the reference RE model (horizontal black dotted line) without any mixing. The explanation for these flux profiles mirrors the discussion of Figure 6 in Section 4.1. At high pressures, the flux is controlled by the radiative flux along the adiabat. Increasing or decreasing the mixing with depth has little effect on the deep eddy flux. Changes to K_{zz} are compensated by $(1 - \nabla/\nabla_{\text{ad}})$ —see Equation (20)—which is small and sensitive to slight changes in ∇ close to the adiabat.

The flux in the low pressure, isothermal region scales as $-F_{\text{eddy}} \propto \rho K_{zz} \propto P^{1+\zeta}$ (see Equation (20)). This explains why the flux components, $F_{\text{rad}} = -F_{\text{eddy}}$, increase with height if $\zeta < -1$. Driving larger radiative fluxes in the upper atmosphere

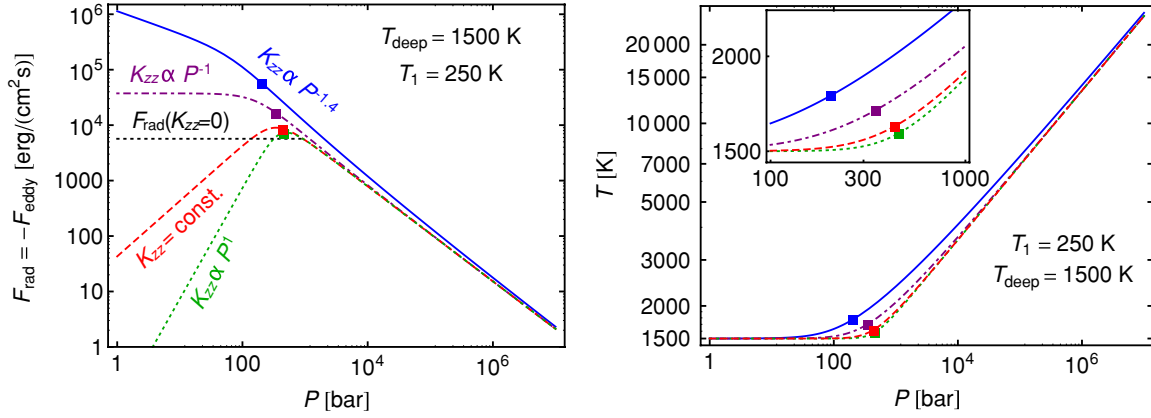


Figure 7. Models with a depth-dependent $K_{zz} \propto P^{-\zeta}$ for $\zeta = 1, 0, -1$, and -1.4 (dotted green, dashed red, dot-dashed purple, and solid blue curves, respectively) and no dissipation. Strong mixing pushes $P_c \rightarrow \infty$ while P_{deep} is plotted with colored squares. Top: radiative flux, which is equal and opposite to the eddy flux. Lower ζ values give strong mixing and larger fluxes at the top of the atmosphere. Bottom: thermal profiles show that strong upper atmosphere mixing (low ζ) heats the upper atmosphere and results in a more gradual approach to the adiabat.

(A color version of this figure is available in the online journal.)

requires a steeper dT/dP . The temperature profiles in Figure 7 (bottom panel) reflect this. The $\zeta = -1$ and especially the top $\zeta = -1.4$ curves are noticeably hotter at intermediate pressures and have smaller P_{deep} . We thus find that mixing at the top of the atmosphere is more effective—compared to uniform or bottom-focused mixing—at lifting (i.e., heating) the T - P profile. The additional heat in this case is provided by a downward flux of mechanical energy across the top boundary.

4.2.1. Limits on Mixing Near the Photosphere

We now consider what might constrain K_{zz} near the top of the atmosphere, since we find that the internal entropy mostly constrains diffusion near P_{deep} . Our $\zeta \leq -1$ solutions in Figure 7 show that strong mixing at the top requires a large flux of mechanical energy at the top of the atmosphere. Weather-layer winds are a plausible source of mechanical energy, and they are generated by the atmospheric heat engine driven by insolation. The thermodynamic efficiency of all planetary atmospheres in the solar system is of order 1%. If we restrict the magnitude of F_{eddy} to a fraction f_* $\sim 1\%$ of the insolation $F_* \sim \sigma T_{\text{deep}}^4$, we get

$$K_{zz,\text{top}} < \frac{f_* F_*}{\rho_{\text{top}} g} \approx 10^9 \frac{\text{cm}^2}{\text{s}} \left(\frac{P_{\text{top}}}{0.1 \text{ bar}} \right)^{-1} \left(\frac{T_{\text{deep}}}{1500 \text{ K}} \right)^5 \frac{f_*}{1\%}, \quad (33)$$

scaled for a downwelling flux that originates at a 0.1 bar photosphere. While the efficiency f_* and mechanisms of generating a downward mechanical flux are uncertain, the energetic difficulties of mixing at $K_{zz} \gg 10^9 \text{ cm}^2 \text{ s}^{-1}$ are evident.

Alternatively, we could attempt to constrain mixing in the upper atmosphere by appealing to our $\zeta = -1.4$ solution. This gives the largest downward eddy flux (Figure 7, top). Smaller ζ values would be needed for a larger flux, but these do not give consistent solutions. In Appendix A, we analyze the $\zeta \approx -1.4$ limit and argue that it may not be physically significant. Ignoring this concern, the diffusion near the top of our $\zeta = -1.4$ solutions is $K_{zz} \approx 5 \times 10^7 (P/\text{bar})^{-1.4} \text{ cm}^2 \text{ s}^{-1}$. A larger internal entropy could support a larger K_{zz} (as we showed for constant K_{zz} models in Figure 4). Therefore, this constraint is not inconsistent with Equation (33), which is a more robust constraint.

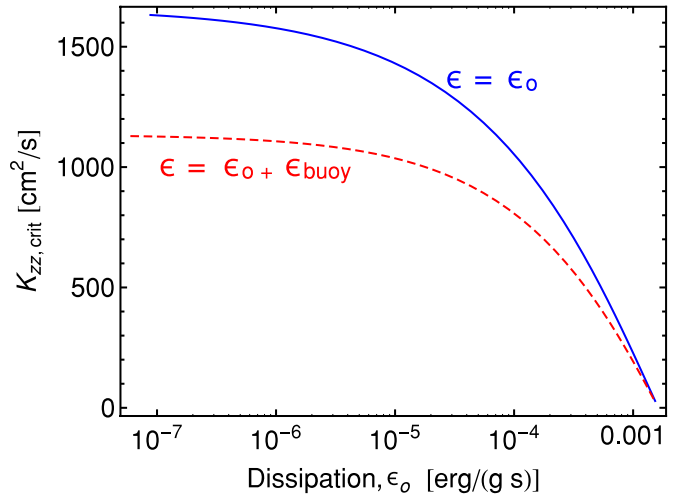


Figure 8. Increasing dissipation reduces $K_{zz,\text{crit}}$, shown for fixed $T_{\text{deep}} = 1500 \text{ K}$ and $T_1 = 250 \text{ K}$. The solid blue curve only includes a constant floor to the dissipation, ϵ_o , while the dashed red curve also includes our prescription for dissipation in stratified regions.

(A color version of this figure is available in the online journal.)

4.3. Including Dissipation

We now consider the effect of adding dissipation to our models with eddy diffusion. The total flux F will now increase with height due to dissipation. The coupled Equations (23) and (24) govern the steady state structure. To understand the effect of dissipation on the turbulent heat flux, we return to the simpler case of spatially uniform K_{zz} .

With dissipation we still find an upper limit to diffusion, $K_{zz,\text{crit}}$, for a given T_1 and T_{deep} . However, $K_{zz,\text{crit}}$ declines with increasing dissipation. Figure 8 shows this for both a dissipation rate ϵ_o that is constant with height (solid blue curve) and the full dissipation prescription (dashed red curve; see Equation (31)). The full prescription includes ϵ_{buoy} , our estimate of the minimum dissipation due to stratified turbulence. This additional dissipation further reduces $K_{zz,\text{crit}}$.

We confirm that the dissipation-free estimates of $K_{zz,\text{crit}}$ in previous sections represent a conservative upper bound. Lowering $K_{zz,\text{crit}}$ means that weaker turbulent diffusion will

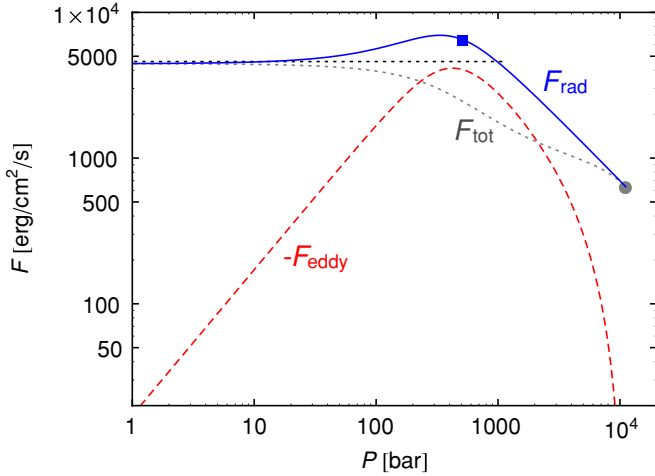


Figure 9. Similar to Figure 6 except dissipation is included. The total flux is no longer constant and the core flux is larger. Both of these effects reduce the magnitude of F_{eddy} which can no longer offset as much of F_{rad} . Consequently, $K_{zz,\text{crit}}$ is reduced to $900 \text{ cm}^2 \text{ s}^{-1}$. The dissipation profile $\epsilon = \epsilon_o + \epsilon_{\text{buoy}}$ includes a floor $\epsilon_o = 5 \times 10^{-5} \text{ erg/(gs)}$ that corresponds to $f_\epsilon = 0.01$, i.e., weaker dissipation near the RCB than in stratified regions.

(A color version of this figure is available in the online journal.)

inflate the planet. Admittedly, the cases shown in Figure 8 do not prove that all dissipation profiles will lower $K_{zz,\text{crit}}$. However, we investigated the effects of both spatially varying K_{zz} (as in Section 4.2) and also different profiles of ϵ . In all cases, adding dissipation reduced $K_{zz,\text{crit}}$ from the dissipation-free value.

4.3.1. How Dissipation Lowers $K_{zz,\text{crit}}$

We explore the energetics of how dissipation lowers $K_{zz,\text{crit}}$. Figure 9 shows the flux balance with dissipation and can be compared to Figure 6. Note that the peak value of $-F_{\text{eddy}}$ now falls well short of F_{rad} at the relevant pressure, P_{deep} . This is because the total flux

$$F = F_c + \int_P^{P_c} \frac{\epsilon}{g} dP \quad (34)$$

now includes the integrated dissipation, causing F to greatly exceed F_c , the small loss of heat from the core. From the RCB to P_{deep} , F_{rad} also increases with height. This rise is not significantly affected by dissipation, with $F_{\text{rad}} \propto P_c^{-6/7}$ along the pseudo-adiabat as before. The magnitude of $-F_{\text{eddy}} = F_{\text{rad}} - F$ is smaller at P_{deep} because dissipation increases F without comparably increasing F_{rad} .

We find that P_{deep} (and also ρ_{deep}) does not significantly change when we add dissipation. Indeed, the T - P or ∇ profiles for the solution in Figure 6 are indistinguishable from the stirred atmospheres in Figure 5, except the RCB is not pushed as deep, “only” to $P_c \approx 11 \text{ kbar}$.

The limiting value of $K_{zz} = 2|F_{\text{eddy}}|/(\rho_{\text{deep}}g)$ drops because the smaller eddy flux is not compensated by a lower ρ_{deep} . It seems possible that some dissipation profile could heat the atmosphere and lower P_{deep} and ρ_{deep} enough to increase $K_{zz,\text{crit}}$. We did not find this to be the case. One reason is that too much dissipation can affect the location of the RCB, a subject we address below.

For completeness, we explain the flux balance at small pressure illustrated in Figure 9. The decline in $-F_{\text{eddy}} \approx \rho g K_{zz}$ with height in isothermal regions again results from declining density. However, F_{rad} does not decline toward low pressure

(as shown in Figure 6), because the total flux F is larger with dissipation. The fact that the escaping flux matches the flux from the RE solution (dotted black line) is a coincidence (with some significance, see below). This coincidence occurs because the dominant dissipation is $\epsilon \approx \epsilon_{\text{buoy}}$. Larger or smaller choices of dissipation would give a larger or smaller (respectively) net F and escaping F_{rad} .

This coincidence has some significance. Downward eddy fluxes reduce the loss of heat from the core, as we have discussed extensively. However, we now see that this loss is matched by the flux due to the dissipation of that turbulence—provided our prescription for the minimum ϵ_{buoy} is correct. This replacement is intriguing, but does not alter our discussions of evolutionary consequences: turbulent dissipation in radiative regions is powered not by interior heat, but by external means (such as forced atmospheric circulation).

4.3.2. The Effect of Dissipation on the RCB

Ignoring dissipation, we obtained the limiting $K_{zz,\text{crit}}$ as $P_c \rightarrow \infty$. With dissipation, $K_{zz,\text{crit}}$ occurs at finite P_c , provided there is dissipation at the RCB. As noted above, the RCB occurs at 11 kbar with $K_{zz} = K_{zz,\text{crit}}$ in Figure 9. Appendix B derives the relation between dissipation and the maximum P_c in Equation (B3).

We consider it physically desirable to restrict P_c to finite pressures. Infinite P_c obviously violates some of our idealizations, notably the plane-parallel and ideal gas approximations. It is encouraging that dissipation alters P_c without qualitatively changing the insights (namely, $K_{zz,\text{crit}}$) gleaned from the non-dissipative model.

Restricting P_c to finite values was not crucial for the energetic balance arguments above. Though F_c is larger for smaller P_c , it is still too small to be the main factor that limits the eddy flux.

To illustrate some of these points, consider the case $\epsilon = \epsilon_{\text{buoy}}$, i.e., with no floor, ϵ_o , to the dissipation. In this case, there is no dissipation at the RCB, and we find that eddy diffusion can still push $P_c \rightarrow \infty$. Nevertheless ϵ_{buoy} by itself does still lower $K_{zz,\text{crit}}$ by $\sim 1/3$. This can be seen in the $\epsilon_o \rightarrow 0$ limits (i.e., the left of the plot) of Figure 8.

4.4. Varying the Opacity Law and EOS

All of our plots and numerical estimates have used an opacity law $\kappa \propto P$ and an ideal gas EOS with $\nabla_{\text{ad}} = 2/7$. We provide general scalings for many results to show the effect of varying these parameters.

Our qualitative results hold for all “reasonable” choices of power-law opacities and EOS. As discussed in Section 2.1, reasonable means that $\nabla_\infty > \nabla_{\text{ad}}$ and $\alpha > -1$ so that RE solutions become convectively unstable at depth. We tested our results with an alternate opacity law $\kappa \propto T^2$ ($\alpha = 0$ and $\beta = 2$) that approximates H^- opacities for $T > 2000 \text{ K}$ or dust grain opacities at colder temperatures. Like $\kappa \propto P$, this law also has $\nabla_\infty = (1 + \alpha)/(4 - \beta) = 1/2 > \nabla_{\text{ad}}$.

The behavior of $K_{zz,\text{crit}}$ —shown in Equation (32)—is particularly important for interpreting our results. The scaling with internal entropy is quite steep with $K_{zz,\text{crit}} \propto T_1^{10.5}$ and $K_{zz,\text{crit}} \propto T_1^7$ for our standard and alternate opacities, respectively. Generally, the entropy dependence becomes steeper for larger α (as in the above example) and also for a smaller ∇_{ad} , but does not depend on β . Recall that the burial of the turbulent heat flux into the convective interior can bring an atmosphere with $K_{zz} > K_{zz,\text{crit}}$ toward energetic equilibrium. A steeper

dependence of $K_{zz,crit}$ on entropy means that less inflation is needed to enforce this equilibrium.

The scaling of $K_{zz,crit}$ with T_{deep} controls how our inflation mechanism depends on the level of irradiation. Also, the development of thermal inversions will lower T_{deep} for a fixed level of irradiation. We find $K_{zz,crit} \propto T_{deep}^{-5.5}$ or $K_{zz,crit} \propto T_{deep}^{-4}$ again for the standard and alternate opacities, respectively. The T_{deep} dependence becomes more steeply negative for larger α (again the dominant effect in our example) and also for larger β (less important in our example) and smaller ∇_{ad} .

These scalings emphasize that a more detailed treatment of turbulent heat fluxes in hot Jupiters should include realistic opacities and EOSs. Non-power-law behavior could have significant consequences. For instance, Guillot et al. (1994) demonstrated the importance of an opacity window near ~ 2000 K. This window can give rise to an isolated convective layer sandwiched between two radiative zones. It would be interesting to consider how a downward turbulent heat flux would interact with such a region. Future work that generalizes our self-similar approach can address these more detailed issues.

5. COMPARISON WITH PREVIOUS WORK

5.1. Simulations of Atmospheric Circulation

Hydrodynamic simulations of hot Jupiter atmospheres have been studied in local (Burkert et al. 2005; Li & Goodman 2010, hereafter LG10) and global (e.g., Cooper & Showman 2005; Rauscher & Menou 2010; Showman et al. 2009b; Dobbs-Dixon & Lin 2008) models. A major goal of these studies is to determine the circulation induced by stellar irradiation. We first discuss estimates of K_{zz} from these simulations and then address the question of whether radiatively forced turbulence extends throughout the radiative zone, as we have assumed. Other sources of turbulence—perhaps involving magnetic fields—may also exist, but we do not analyze them here.

The global circulation models (GCMs) of Showman et al. (2009b) estimate $K_{zz} \sim 10^{11} \text{ cm}^2 \text{ s}^{-1}$ at mbar pressures. This does not contradict our constraint on upper atmospheric mixing from the efficiency of radiative forcing (Equation (33)) when extrapolated to such low pressures. Moreover, at low pressures radiative losses can lower the eddy flux (see Section 3.1) and further weaken our constraint on K_{zz} . We caution that K_{zz} estimates from GCMs are rough, since they only resolve relatively large scale flow patterns. The Showman et al. (2009b) K_{zz} estimate arises from multiplying measured vertical speeds by the scale height H . While a useful guide to what is possible, this does not constitute a direct measurement of diffusion.

Local hydrodynamic simulations can better resolve turbulent flows, though as usual with Reynolds numbers far lower than reality. The calculations of LG10 find an effective turbulent viscosity of $\nu_t \sim 0.001\text{--}0.01 c_s H \sim 10^{10}\text{--}10^{11} \text{ cm}^2 \text{ s}^{-1}$. It is unclear if this viscosity should be interpreted as a mixing coefficient. Their simulation with $\nu_t = 0.015 c_s H$ has an rms vertical speed $w \sim 0.3 c_s$. Thus, assuming $\nu_t \sim K_{zz}$ is not consistent with the simple estimate $K_{zz} \sim w\ell$ because it gives a length scale $\ell \sim H/20$, smaller than the grid spacing of $H/10$. It should not be surprising that simple estimates based on three-dimensional isotropic turbulence fail, given the organized structure in their two-dimensional “turbulent” state.

Moreover, the forcing in LG10 was not by irradiation, but chosen to be large enough to drive super-sonic flows despite artificial viscosities that are large for numerical reasons. Thus, attempting to interpret the Carnot efficiency of stellar irradiation

may overextend their results. Despite these caveats, if the LG10 simulations apply near the millibar weather layer, there is again no contradiction with Equation (33).

Global simulations indicate that the shear layer may not extend throughout the radiative zone. For instance, Showman et al. (2009b) find that strong ($\sim \text{km s}^{-1}$) zonal winds terminate at ~ 10 bar. They argue that circulation stops because the planet is horizontally isothermal at these depths, removing the local forcing. However, hot Jupiter atmospheres have a large separation between the radiative timescales in the weather layer and the deep radiative layer. It is possible (and arguably likely) that unresolved or long timescale dynamics could push the shear layer even deeper. This possibility should be explored in future modeling studies.

How far turbulence can extend below the shear layer is also uncertain. LG10 force a shear layer of with $\sim 2H$, but find that turbulence (or at least some disordered motion) extends throughout their box of size $\sim 5H$ (see their Figure 10). Turbulence that extends a full $5H$ below a shear layer could thus extend to $P \sim e^5 \cdot 10 \text{ bar} \sim 1.5 \text{ kbar}$. These issues deserve further study, but it cannot be ruled out that the radiative zone is turbulent down to the RCB.

5.2. Thermal Inversions via TiO Diffusion

We now provide a more detailed interpretation of our results in terms of the S09 constraints on the mixing required to loft TiO and create thermal inversions. We emphasize that the constraints on K_{zz} and especially on the depth dependence of K_{zz} depend sensitively on whether or not there is a cold trap. Wherever TiO condenses, one must consider the mixing of dust grains, not just molecules.

First, consider the case where there is no cold trap, and TiO is always in the vapor phase. In the S09 analysis, this is only possible for the most intensely irradiated planet, WASP 12b, in part because thermal inversions lower T_{deep} and favor condensation at depth. The mixing of TiO vapor requires $K_{zz} \sim 10^7 \text{ cm}^2 \text{ s}^{-1}$ at $P \sim 1 \text{ mbar}$, i.e., the height of the inversion where TiO is needed. The specification of pressure level is important because the constraint on molecular diffusion scales as $K_{zz} \propto P^{-1}$ in an isothermal atmosphere. Thus, the constraint is weaker at depth. In a model where the actual $K_{zz} \propto P^{-1}$ (as in Section 4.2), we only require $K_{zz} \sim 10 \text{ cm}^2 \text{ s}^{-1}$ at the kbar RCB. In this case, our model predicts a minimal effect of the eddy flux on the planet’s evolution, though the dissipation of turbulence above the RCB could still be significant.

We briefly summarize how this $K_{zz} \sim 10^7 \text{ cm}^2 \text{ s}^{-1}$ limit and the depth dependence arise, and refer the reader to S09 for details. With only molecular viscosity, i.e., collisions, the TiO scale height would be hydrostatic, and thus ~ 30 times smaller than the dominant H_2 species. S09 conclude that the turbulent diffusion must exceed the molecular diffusion D_{TiO} by a factor ~ 100 , due to the many (~ 14) scale heights between $P \sim \text{mbar}$ and the kbar RCB. Estimating D_{TiO} as usual—the product of the mean free path and thermal speed—gives an inverse scaling with density, and thus also with pressure in isothermal regions. The numerical value of $D_{\text{TiO}} \sim 10^5 \text{ cm}^2 \text{ s}^{-1}$ at $P \sim \text{mbar}$, combined with the factor of 100 excess needed for efficient turbulent mixing, gives the $K_{zz} \sim 10^7 \text{ cm}^2 \text{ s}^{-1}$ constraint.

Now consider the case where grains do condense somewhere in the radiative zone, which is true for most hot Jupiters (especially those with inversions). The K_{zz} required to loft TiO increases to $10^8\text{--}10^{11} \text{ cm}^2 \text{ s}^{-1}$ depending on the size of grains and the depth of the cold trap. A rough estimate of

$K_{zz} \sim v_{\text{term}}L$ follows from equating the diffusion timescale, L^2/K_{zz} , to the dust settling timescale L/v_{term} , where L is the depth of the cold trap and v_{term} the grain's terminal speed. While the terminal speed will increase with particle size, it does not depend on atmospheric density for the relevant viscous (i.e., Stokes') drag. Thus, unlike the case of molecular viscosity, the K_{zz} required for mixing condensed grains does not decline with depth.

We can thus conclude that the K_{zz} required to mix TiO and create thermal inversions in a hot Jupiter are likely excessive, provided TiO condenses somewhere in the radiative zone. This follows from Figure 4 which shows that $K_{zz} \sim 10^9 \text{ cm}^2 \text{ s}^{-1}$ appear off-scale. The internal (specific) entropy of a planet would have to increase by $\gtrsim 2k_B/m_p$ for a planet with $T_{\text{deep}} \gtrsim 1500 \text{ K}$, as is the case for all planets in S09. It seems likely that such large entropies would overinflate a planet, based on studies such as in AB06. This is especially true because Figure 4 neglects dissipation which can further inflate a planet, which can occur by lowering $K_{zz,\text{crit}}$ as shown in Figure 8.

However, we cannot firmly declare that the TiO hypothesis fails. This is largely due to the approximate nature of our treatment of opacities and the EOS. A more conclusive analysis of the TiO hypothesis would require a detailed atmospheric model that includes the eddy fluxes and turbulent dissipation described in this work. Such a study would also have to abandon the fixed flux bottom boundary condition used in most atmospheric models (including S09). Instead, the bottom boundary should be a fixed adiabat, chosen to match the observed radius. This is subject as usual to assumptions about composition and presence of a core. However, allowing the flux to float is needed for a consistent determination of the RCB. This is crucial for understanding the coupled relationship between compositional mixing and cooling history.

6. CONCLUSIONS

6.1. Summary of Results

We have investigated how forced turbulent mixing affects the energetic balance and structure of the stably stratified, radiative layers of hot Jupiters. It is crucial to understand how the radiative layer matches onto the convective interior at the RCB. This regulates the rate at which the planet cools and therefore controls the evolution of the planet's radius.

Previous work has invoked turbulent eddy diffusion of molecular species (and dust). This mixing changes the opacity to provide better-fitting model spectra of transiting planets, especially those that appear to have thermal inversions (S09). We find that turbulent mixing of this kind does not just redistribute chemical species but also significantly affects energetics.

Forced turbulent mixing in stable, radiative regions drives a downward flux of energy that pushes the RCB deeper in the atmosphere, lowering the planet's cooling rate. We found an upper limit to the strength of turbulent diffusion, $K_{zz,\text{crit}}$, that can be achieved in steady state. Beyond this limit, the downward flux of energy will heat the convective interior and inflate the planet. We did not directly model this entropy growth because our model was steady state and did not include overshoot across the RCB. The deep, marginally stable layer in our solutions would not strongly inhibit overshoot, so heat burial by this mechanism is a likely outcome. Our solutions indicate that interior heating brings the planet back toward steady state, because higher entropy planets have larger $K_{zz,\text{crit}}$ (see Figure 4). Our mechanism is thus a “mechanical greenhouse effect” with

the role of sunlight in the traditional greenhouse being played by forced turbulent mixing.

For non-uniform turbulent mixing, we find that our constraint on $K_{zz,\text{crit}}$ applies near the RCB. More specifically, this constraint applies at a pressure P_{deep} , which lies below the deep isothermal region where the radiative layer is transitioning toward convective instability. Our constraints on turbulence in the upper atmosphere are less stringent. However, the downward flux of mechanical energy likely cannot exceed a small fraction (probably at the percent level) of the stellar irradiation if it is supplied by weather-layer winds. If turbulence is too weak at the bottom of the radiative layer, it will not dredge up heavy molecular species—particularly those that condense onto dust grains—to serve as opacity sources near the observable photosphere.

Turbulence also deposits heat in the radiative atmosphere when it decays. Non-turbulent sources of energy dissipation—including nonlinear wave breaking and ohmic dissipation—also affect energetic balance. We find that including energy dissipation reduces $K_{zz,\text{crit}}$, and thus makes it easier to inflate a planet for a given level of forced turbulence.

We find a characteristic scale of $K_{zz,\text{crit}} \sim 10^3\text{--}10^5 \text{ cm}^2 \text{ s}^{-1}$ for typical hot Jupiter parameters, even ignoring dissipation. This is orders of magnitude below values quoted in the literature of $10^7\text{--}10^{11} \text{ cm}^2 \text{ s}^{-1}$ for the mixing of chemical species (Spiegel et al. 2009; Zahnle et al. 2009). We caution that our quantitative results should be taken as illustrative, due to the approximations detailed in Section 2.

Thus, when turbulence is important for the redistribution of opacity sources, it also has significant energetic consequences. Our model represents a step toward more self-consistent modeling of exoplanet atmospheres.

6.2. Applications and Extensions

Guillot & Showman (2002) first noted that dissipation in radiative layers can slow planetary contraction by pushing the RCB to higher pressures. They imagined dissipation concentrated in the upper regions of the atmosphere, sourced by insolation driven winds. Other authors (e.g., Bodenheimer et al. 2003) have included the Guillot & Showman (2002) dissipation prescription to model exoplanet radii.

However, we are unaware of previous works that include the mechanical flux of energy due to turbulence or waves—our F_{eddy} —in radiative layers. Incorporating this effect in detailed planetary evolution models would require a more precise treatment than this exploratory study. Notably it would require a global model with a realistic EOS and opacity, not the power laws considered here.

In this paper, we treat diffusion and dissipation by forced turbulence as free parameters to allow a general analysis. This approach is justified since we currently lack a detailed understanding of these processes. Thus, our model can be used to test how any specific model for turbulence and/or energy dissipation affects the structure and evolution of the planet. For instance, the work of Batygin & Stevenson (2010) considers ohmic dissipation in radiative and convective regions, but does not recompute the effect of the dissipation on the structure of the radiative layer. Our point is not to critique, but to emphasize that a more consistent treatment of energetics may make it easier to inflate a planet—by any number of mechanisms.

We also hope to include the effects of our study in detailed three-dimensional radiation-hydrodynamical simulations of exoplanet atmospheres. This would involve adding sub-grid

physical prescriptions for eddy fluxes to GCMs such as those by Showman et al. (2009b) and Rauscher & Menou (2010) and/or non-hydrostatic simulations (Dobbs-Dixon et al. 2010). Goodman (2009) discusses the need to include explicit sources of dissipation. Li & Goodman (2010) present a first step toward sub-grid modeling of turbulence due to Kelvin–Helmholtz instabilities. Breaking of vertically propagating gravity waves represents another possible source of turbulence (Showman et al. 2009a). When all these effects are taken into account, the inflated radii of transiting planets may not be surprising after all.

We have focused on hot Jupiters, but the physics we describe in principle applies to other atmospheres. Our limits on eddy diffusion become less severe as objects are more weakly irradiated (see Figure 4). Thus, our mechanism would not inflate longer period gas giants, including Jupiter and Saturn. More intrinsically luminous objects like brown dwarfs will similarly be less affected. The expanding inventory of transiting exoplanets, at wider separations, is an excellent test of radius evolution models.

Finally, we comment on a possible connection to the atmosphere of Venus. Venus has a marginally stable pseudo-adiabat beneath a thick cloud deck (Schubert et al. 1980). The clouds shield sunlight from warming the surface of Venus. Because of this, Venus’ atmosphere would be nearly isothermal were it not for some poorly understood mechanical stirring process. Our well-stirred hot Jupiter atmospheres also have marginally stable pseudo-adiabats at depth. Perhaps Venus is a very well-stirred analog of a hot Jupiter. Obvious differences exist, for instance, the non-negligible fraction of sunlight that reaches the Venusian surface versus the radiant flux escaping the core of hot Jupiters. Pursuing analogies such as these should improve our understanding of worlds near and far.

A.N.Y. and J.L.M. thank David Spiegel for extensive discussions and Peter Goldreich for wise counsel. A.N.Y. thanks William Hubbard and Roger Yelle for insights into planetary cooling and eddy diffusion, respectively. J.L.M. thanks Martin Pessah and Shane Davis for helpful discussions. J.L.M. and A.N.Y. thank the Institute for Advanced Study for hosting them during the early stages of this work. This research was supported in part by the National Science Foundation under grant No. PHY05-51164 for A.N.Y. to visit the KITP. A.N.Y. thanks Travis Barman, Lars Bildsten, Brad Hansen, and Emily Rauscher for useful feedback during the KITP program “The Theory and Observation of Exoplanets.” We thank the anonymous referee and Kristen Menou, David Spiegel, Tristan Guillot, and David Stevenson for comments that improved the submitted manuscript.

APPENDIX A

ZERO FLUX SOLUTIONS

In addition to the solution technique described in Section 3.2, we also used a more specialized technique that applies to a reduced model with no dissipation and a net flux $F = 0$. As we show in Section 4.1, this is an interesting case because the downward flux of heat can drive the core flux, $F_c \rightarrow 0$, and the flux remains zero in the absence of dissipation. This alternate technique allows us to check our results. It allows integration from the top down, compared to the bottom up integration from the RCB (which recedes to infinite pressure for the zero flux solution). We do not need to specify the parameter ψ_c (Equation (26)), which diverges for these zero flux solutions.

With the reduced model, we can analytically explore solution properties. We will do this below to explain why we cannot obtain solutions with $\zeta \lesssim -1.5$ in Section 4.2.

Ignoring dissipation and setting $F = 0$, we can rearrange Equation (23) as

$$\frac{dT}{dP} = \nabla_{\text{ad}} \frac{T}{P} \left(1 + \frac{\nabla_{\text{ad}} k_{\text{rad}} T}{\rho g K_{zz} P} \right)^{-1}. \quad (\text{A1})$$

We can integrate from $P = 0$ with the boundary condition $T(0) = T_{\text{deep}}$. The solutions approach an adiabatic profile $T \propto P^{\nabla_{\text{ad}}}$ at large pressure (shown below). One could find solutions by integrating with various K_{zz} values, iterating until one lands on a desired adiabat. Instead we again take a self-similar approach, non-dimensionalizing the pressure using K_{zz} and the opacity law. We choose a physical scale for the pressure by matching the self-similar solution onto a chosen adiabat. This fixes the value of K_{zz} (at a reference pressure if K_{zz} is not uniform). The special value of K_{zz} that gives a zero flux solution for a given adiabat is the limiting $K_{zz, \text{crit}}$ discussed in Section 4.1.

We now show that the solution to Equation (A1) becomes adiabatic at large pressure, at least if K_{zz} is constant. If the final term in the parentheses vanishes we have $\nabla \rightarrow \nabla_{\text{ad}}$. We can show that an adiabatic solution is consistent by assuming $T \propto P^{\nabla_{\text{ad}}}$ and then confirming that the final term

$$\frac{\nabla_{\text{ad}} k_{\text{rad}} T}{\rho g K_{zz} P} \propto \frac{T^{5-\beta}}{P^{2+\alpha}} \propto P^{(2+\alpha)(\nabla_{\text{ad}}/\nabla_{\infty}' - 1)} \ll 1 \quad (\text{A2})$$

as $P \rightarrow \infty$. With $\nabla_{\infty}' \equiv (2 + \alpha)/(5 - \beta)$, we can show that the exponent in the last proportionality of Equation (A2) is indeed negative. This is because $\nabla_{\infty}' > \nabla_{\infty}$ (which is generally true, for our opacity $\nabla_{\infty}' = 3/5 > 1/2$) and because reasonable opacities have $\alpha > -1$ and $\nabla_{\infty} > \nabla_{\text{ad}}$ (see Section 2). Thus, a deep adiabat is a consistent solution at large pressure, for constant K_{zz} .

Now consider a spatially varying $K_{zz} \propto P^{\zeta}$. In this case, the assumption of an adiabat at depth gives

$$\frac{\nabla}{\nabla_{\text{ad}}} \rightarrow \frac{1}{1 + c_{\zeta} P^{e_{\zeta}}} \quad (\text{A3})$$

as $P \rightarrow \infty$, where c_{ζ} is constant and $e_{\zeta} = \nabla_{\text{ad}}(5 - \beta) - (2 + \alpha + \zeta)$. Consistency (i.e., $\nabla \rightarrow \nabla_{\text{ad}}$) requires that $e_{\zeta} < 0$ or $\zeta > -(2 + \alpha) + \nabla_{\text{ad}}(5 - \beta) = -11/7 \approx -1.57$. More negative values of ζ do not approach an adiabat even at infinite pressure.

This explains the behavior of the $\zeta \lesssim -1.4$ solutions in Section 4.2. However, we should not overinterpret the physical significance of this result since it may merely reflect a limitation of the self-similar approach. More study is needed of what happens when a large mechanical flux of energy enters the top of the atmosphere, but turbulent heat burial is very weak near the RCB (which is the case for negative ζ). For the time being, we thus consider the irradiation efficiency constraint in Equation (33) as our best limit on turbulent mixing in the upper atmosphere.

APPENDIX B

MAXIMUM DISSIPATION AT RCB

This appendix derives how dissipation at the RCB restricts the RCB depth P_c . We use the consistency requirement that

$d\nabla/dP \geq 0$ at the RCB. This states that the solution will indeed be convectively stable above the RCB. We rearrange Equation (23) to give

$$\frac{\nabla}{\nabla_{\text{ad}}} = \frac{F + F_{\text{iso}}}{\nabla_{\text{ad}} k_{\text{rad}} T/P + F_{\text{iso}}} \quad (\text{B1})$$

and at the RCB (denoted by the ‘‘c’’ subscript) we have $F = F_c = \nabla_{\text{ad}}(k_{\text{rad}}T/P)_c$. The gradient of ∇ at the RCB is

$$\frac{d}{dP} \left(\frac{\nabla}{\nabla_{\text{ad}}} \right)_c = \frac{1}{F_c + F_{\text{iso},c}} \frac{d}{dP} \left[F - \frac{\nabla_{\text{ad}} k_{\text{rad}} T}{P} \right]_c, \quad (\text{B2})$$

where the derivatives of F_{iso} cancel. Thus, the limit on dissipation at the RCB, using Equation (18) and requiring $(d\nabla/dP)_c \geq 0$, is

$$\epsilon_c \leq (1 + \alpha) \left(1 - \frac{\nabla_{\text{ad}}}{\nabla_{\infty}} \right) \frac{F_c g}{P_c} = \frac{6F_c g}{7P_c}. \quad (\text{B3})$$

Since $F_c/P_c \propto P_c^{-11/7}$, the maximum depth of the RCB declines with increasing dissipation at the RCB.

This result is very useful in finding $K_{zz,\text{crit}}$ values with dissipation. Without dissipation we could easily find $K_{zz,\text{crit}}$ by increasing ψ_c (Equation (26)) to arbitrarily large values (which results in Figure 3), or by using the zero flux solutions of Appendix A. Instead we add a twist to the self-similar technique of Section 3.2. We set the dissipation at the RCB to the limiting value of Equation (B3). We further assume that the dissipation is of the form of Equation (30) so that the strength of the dissipation is set by the dimensionless f_ϵ . We have thus coupled dissipation to K_{zz} mathematically. (It does not matter if they are unrelated physically, since f_ϵ can be adjusted to give any desired level of dissipation.) Then, we can solve Equations (26), (29), (30), and (B3) for

$$\psi_c = \frac{6T_{\text{deep}}}{7f_\epsilon \nabla_{\text{ad}} T_c}. \quad (\text{B4})$$

Since T_c is not known until we obtain a solution, we use an iteration procedure: guess a value for T_c (but start with something too low), use the estimate of ψ_c from Equation (B4) to integrate the model Equations (23) and (24), use the resulting T_c to refine ψ_c and repeat. Though a bit convoluted, this procedure converges.

Finally, note that our constraint on dissipation at the RCB does not ensure stability at all $P < P_c$. Assume that the inequality in Equation (B3) holds so that there is a radiative layer above

the RCB. Dissipation could still create another convective layer at greater height. However, our self-similar solutions cannot include such structures. Thus, we leave it to a future work to consider these more complicated scenarios and their effects on planetary evolution.

REFERENCES

- Arras, P., & Bildsten, L. 2006, *ApJ*, **650**, 394 (AB06)
- Baraffe, I., Chabrier, G., Barman, T. S., Allard, F., & Hauschildt, P. H. 2003, *A&A*, **402**, 701
- Batygin, K., & Stevenson, D. J. 2010, *ApJ*, **714**, L238
- Bodenheimer, P., Laughlin, G., & Lin, D. N. C. 2003, *ApJ*, **592**, 555
- Burkert, A., Lin, D. N. C., Bodenheimer, P. H., Jones, C. A., & Yorke, H. W. 2005, *ApJ*, **618**, 512
- Burrows, A., Guillot, T., Hubbard, W. B., Marley, M. S., Saumon, D., Lunine, J. I., & Sudarsky, D. 2000, *ApJ*, **534**, L97
- Burrows, A., Hubeny, I., Budaj, J., Knutson, H. A., & Charbonneau, D. 2007, *ApJ*, **668**, L171
- Chabrier, G., Barman, T., Baraffe, I., Allard, F., & Hauschildt, P. H. 2004, *ApJ*, **603**, L53
- Cooper, C. S., & Showman, A. P. 2005, *ApJ*, **629**, L45
- Dobbs-Dixon, I., Cumming, A., & Lin, D. N. C. 2010, *ApJ*, **710**, 1395
- Dobbs-Dixon, I., & Lin, D. N. C. 2008, *ApJ*, **673**, 513
- Fortney, J. J., Baraffe, I., & Militzer, B. 2009, arXiv:0911.3154
- Goodman, J. 2009, *ApJ*, **693**, 1645
- Griffith, C. A., & Yelle, R. V. 1999, *ApJ*, **519**, L85
- Guillot, T. 2010, arXiv:1006.4702
- Guillot, T., Gautier, D., Chabrier, G., & Mosser, B. 1994, *Icarus*, **112**, 337
- Guillot, T., & Showman, A. P. 2002, *A&A*, **385**, 156 (GS02)
- Hansen, B. M. S. 2008, *ApJS*, **179**, 484
- Hubbard, W. B. 1977, *Icarus*, **30**, 305
- Hubeny, I., & Burrows, A. 2007, *ApJ*, **669**, 1248
- Hubeny, I., Burrows, A., & Sudarsky, D. 2003, *ApJ*, **594**, 1011
- Ingersoll, A. P. 1969, *J. Atmos. Sci.*, **26**, 1191
- Iro, N., Bézard, B., & Guillot, T. 2005, *A&A*, **436**, 719
- Knutson, H. A., Howard, A. W., & Isaacson, H. 2010, arXiv:1004.2702
- Kobayashi, M. 1967, *J. Meteor. Soc. Japan*, **45**, 137
- Li, J., & Goodman, J. 2010, arXiv:1005.0589 (LG10)
- Miller, N., Fortney, J. J., & Jackson, B. 2009, *ApJ*, **702**, 1413
- Perna, R., Menou, K., & Rauscher, E. 2010, *ApJ*, **719**, 1421
- Rauscher, E., & Menou, K. 2010, *ApJ*, **714**, 1334
- Richardson, L. J., Deming, D., Horning, K., Seager, S., & Harrington, J. 2007, *Nature*, **445**, 892
- Schubert, G., et al. 1980, *J. Geophys. Res.*, **85**, 8007
- Seager, S., & Sasselov, D. D. 2000, *ApJ*, **537**, 916
- Showman, A. P., Cho, J., & Menou, K. 2009a, arXiv:0911.3170
- Showman, A. P., Fortney, J. J., Lian, Y., Marley, M. S., Freedman, R. S., Knutson, H. A., & Charbonneau, D. 2009b, *ApJ*, **699**, 564
- Spiegel, D. S., Silverio, K., & Burrows, A. 2009, *ApJ*, **699**, 1487 (S09)
- Zahnle, K., Marley, M. S., Freedman, R. S., Lodders, K., & Fortney, J. J. 2009, *ApJ*, **701**, L20